Thermal stability of ultrafine grained copper

Jakub Čížek, Ivan Procházka, Miroslav Cieslar, Radomír Kužel, Jan Kuriplach, František Chmelík, Ivana Stulíková, František Bečvář, and Oksana Melikhova
Faculty of Mathematics and Physics, Charles University, V Holešovičkách 2, CZ-180 00 Prague 8, Czech Republic

Rinat K. Islamgaliev
Institute of Physics of Advanced Materials, Ufa State Aviation Technical University, Ufa 450000, Russia
(Received 15 February 2001; revised manusript received 9 July 2001; published 6 February 2002)

Thermal stability of ultrafine grained (mean grain size 150 nm) copper prepared by high pressure torsion was studied by means of positron-lifetime spectroscopy correlated with transmission electron microscopy. The microstructure of the material studied is strongly inhomogeneous. The grain interiors with low dislocation density are separated by distorted regions with high number of dislocations. We have found that positrons are trapped at dislocations inside the distorted regions and in the microvoids situated inside the grains. Calculations of the lifetime of a positron trapped at a microvoid as a function of its size were performed to obtain information about sizes of the microvoids. Abnormal grain growth, when isolated recrystallized grains grow inside the deformed matrix, takes place from 160 °C. From 280 to 400 °C recrystallization occurs. Strongly inhomogeneous spatial distribution of defects does not allow application of the simple trapping model. Therefore a model of positron behavior in the ultrafine grained materials was developed in the present work. The model takes into account inhomogeneous spatial distribution of defects and allows for determination of dislocation density, concentration of microvoids, linear size of coherent domains, and volume fraction of the distorted regions. Moreover using this model it was possible to determine the activation energy of the recrystallization.

DOI: 10.1103/PhysRevB.65.094106 PACS number(s): 78.70.Bj, 79.60.Jv, 61.72.−y, 61.46.+w

I. INTRODUCTION

Nanocrystalline (NC) materials are polycrystals with the mean grain size below 10 nm.[1] Submicrocrystalline polycrystals with a mean grain size of about 100 nm are often called ultrafine grained (UFG) materials.[2] In recent years the NC as well as the UFG materials have attracted much interest of researchers in the field of materials science. It is connected with new, unusual properties caused by significant volume fraction of grain boundaries (GB's), i.e., interfaces among individual crystallites, in these nontraditional materials. In particular the NC and the UFG materials exhibit abnormally high diffusion activity,[3] unusual changes in Curie temperature, saturation magnetization, and elastic properties,[4] as well as highly strengthened state and high strain rate superplasticity.[5,6]

NC materials can be produced by gas condensation method (GCM).[1,7] A disadvantage of this technique consists in the fact that nanocrystals prepared by the GCM contain gas impurities and residual porosity.[1,8] Recently it has been shown that very fine crystalline structures with a mean grain size from 50 to 200 nm can be achieved by high pressure torsion (HPT).[5,2] The HPT technique leads to specimens with larger grain size, however, it has several advantages. Contrary to the GCM, (i) no residual porosity was found in the samples produced by HPT, (ii) high purity UFG materials can be prepared, and (iii) one can obtain massive samples (sheets, rods).

The investigations of NC materials by means of x-ray diffraction (XRD) have revealed that GB's exhibit highly disordered atom arrangement without short-range order.[1,9] Positron-lifetime (PL) spectroscopy gives detailed information about the open-volume defects. It was used for determination of defects associated with the extraordinary structure of the GB's in NC materials prepared by GCM by a number of authors.[10–13] All these studies have led to the conclusion that ''vacancy-like'' open volume defects with the size of about one missing atom were present in the NC specimens together with larger defects whose size is comparable to a vacancy cluster. A few PL studies of UFG metals prepared by HPT have also been performed[14,15] and similar two defect components were found in PL spectra. However, interpretation of the PL results has to be done with care, because there are significant differences between the microstructure of the NC materials prepared by GCM and the UFG ones prepared by HPT. The UFG materials prepared by HPT exhibit high dislocation density, while dislocations are unstable in the NC materials due to small grain size.[12] In the UFG materials prepared by GCM the dislocations are distributed strongly inhomogeneously, which was confirmed both by transmission electron microscopy (TEM)[16,17,2] and XRD (Ref. 18) measurements. The grain interiors almost free of dislocations are separated by the distorted regions (DR's) with high dislocation density situated along GB's.[2] In order to obtain detailed information about types and concentrations of defects present in the UFG materials prepared by HPT, PL spectroscopy correlated with TEM investigation seems to be very useful.

Investigations of microstructure evolution with increasing temperature in the NC or the UFG materials represent a further important task in the study of these materials. It is interesting from a physical point of view, as information about recovery of strongly nonuniform structure is obtained. The enhanced mechanical properties make the NC and the UFG

materials extremely attractive for technical applications. These advantageous properties are connected with the NC or the UFG structure. Hence, thermal stability of the microstructure of these materials is crucial for their future technical use.

Electrical resistometry, TEM, XRD, and differential scanning calorimetry (DSC) were used in the investigation of the thermal stability of UFG Cu and Ni.[16] This study by different techniques has revealed that there are some recovery processes probably connected with relaxation of elastic stresses and some rearrangement of defect structure inside the DR's,[16] which precede grain growth. These recovery processes prior to grain growth cause a significant decrease of electrical resistivity as well as an exothermal peak in DSC measurement.[16] Significant structure changes at the annealing temperatures prior to grain growth were also confirmed by XRD.[16]

The additional studies of microstructure thermal evolution are necessary for understanding of the processes connected with the recovery of the nonequilibrium UFG structure. In particular there is complete lack of information about thermal evolution of the microvoids in the UFG materials prepared by HPT. Both the mean size and concentration of the microvoids can be relatively easily obtained by PL spectroscopy, while they can hardly be detected by other available techniques. Together with large sensitivity to dislocations, it makes from PL spectroscopy an ideal tool for investigations of the thermal evolution of defects in NC and UFG materials. Several PL investigations of thermal stability of the NC materials prepared by GCM have been performed.[11–13] It was found that the thermal stability of the NC materials prepared by GCM is strongly influenced by the presence of the gas impurities and the residual porosity.[11,19] Essentially no change of the lifetimes and the relative intensities was found for NC Cu up to 400 °C.[12] Similarly no major changes in positron parameters were observed for NC Pd in the range 500–900 °C,[10] although remarkable crystalline growth took place. On the other hand, Eldrup *et al.*,[11] who studied NC Cu of improved purity prepared by GCM, observed a substantial increase of the relative intensity of the component belonging to the microvoids starting from 200 °C. This increase of the relative intensity was accompanied by a slight decrease of the lifetime of positrons trapped in the microvoids. One would expect that the number of the microvoids decreases with the annealing temperature, however the relative intensity indicates the opposite process. There is still no explanation for this surprising behavior. In this connection, it is very interesting to study thermal evolution of the microvoids also in the UFG specimens prepared by HPT and to compare the results with those already obtained on the NC materials prepared by GCM.

The aim of the present work is to use PL spectroscopy correlated with TEM to study the microstructure of UFG Cu prepared by HPT and its evolution with increasing annealing temperature. Our work is focused mainly on nonequilibrium defects present in the material and their recovery. High resolution PL spectroscopy [150 ps full width at half maximum (FWHM) for ^{22}Na] allows for proper determination of even very short and weak components in PL spectra. The results of PL spectroscopy are correlated with TEM, which makes possible direct observation of dislocations and their spatial distribution as well as observation of grain growth.

In the interpretation of experimental PL spectra obtained on the UFG materials highly nonuniform spatial distribution of dislocations must be taken into account. In order to obtain correct values of defect densities from PL spectra we developed in the present work a model of positron trapping in the UFG materials, which directly takes into account the inhomogeneous spatial defect distribution. In the framework of this model, it is possible to determine dislocation density, concentration of the microvoids, the linear size of the coherent domains, and the volume fraction of the DR's. These physical parameters obtained from the model are directly compared with the TEM observations as well as the results of other methods available in literature.

The paper is organized as follows. In Sec. II details about the specimens and techniques of their investigations are given. Obtained results are described in Sec. III A for the as-prepared state. Results regarding evolution of the microstructure with increasing temperature are shown in Sec. III B. Calculations of microvoid size are given in Sec. III C. The model of positron behavior in the UFG materials and its application to the UFG Cu can be found in Sec. IV. In Sec. V a brief comparison of PL results with other nonlocal techniques used in the study of UFG materials is done. Conclusions of the present investigations are summarized in Sec. VI.

II. EXPERIMENTAL DETAILS

A. Specimens

Copper specimens of purity 99.99% were studied. In order to fabricate the UFG structure the specimens were subjected to high pressure torsion under pressure of 3 GPa performed at room temperature. This technique was described in Ref. 20. Microstructure of the as-prepared state of the specimens was investigated by means of TEM and PL spectroscopy. Subsequently, the specimens were subjected to isochronal annealing. Temperature step was 30 °C and specimens were annealed for 30 min at each temperature, i.e., corresponding effective heating rate was 1 °C /min. The annealing was carried in oil base thermostat up to 250 °C and in vertical furnace with protective argon atmosphere above this temperature. Each annealing step was finished by quenching to water of room temperature. Both PL and TEM measurements were performed at room temperature.

B. Positron-lifetime spectroscopy

A PL spectrometer similar to the fast–slow one described in Refs. 21 and 22 was employed in the present work. The spectrometer was modified recently to enhance the coincidence count rate while simultaneously keeping the excellent timing resolution (for details see Refs. 23 and 22). The main improvement with respect to the device[21] consisted in the selection of coincidence events by means of summing the energy signals as described in Refs. 23 and 22. A ^{22}Na positron source of activity of $\sim$1.3 MBq sealed between two

mylar foils of thickness of 2 μm was used. The timing resolution of the spectrometer was 150 ps (FWHM) for ^{22}Na at a typical coincidence counting rate of $\sim 75\ s^{-1}$. At least 10^7 counts were collected in each PL spectrum. Measured spectra were decomposed by means of maximum-likelihood procedure[24] into up to five exponential components. The time-resolution function of the spectrometer was considered as a sum of the three Gaussians and was fitted simultaneously with the other parameters (for details see Refs. 24 and 22).

C. Transmission electron microscopy

Observations of microstructure were performed on the JEOL 2000 FX electron microscope operating at 200 kV with EDX system LINK AN 10000. Thin foils for TEM were electropolished in a twin-jet device TENUPOL 2. The electropolishing was performed in 30% solution of HNO_3 at $-20\,^{\circ}C$. Some specimens were ion milled at TECHNOORG LINDA device in order to remove surface impurities and oxides.

D. X-ray diffraction

X-ray studies were carried out with the aid of XRD7 and HZG4(Seifert-FPM) powder diffractometers using Cu $K\alpha$ radiation filtered with a nickel foil and Soller slits placed in the diffracted beam. XRD profiles were fitted with the Pearson VII function by the program DIFPATAN, see Ref. 25. The lattice parameters were determined by the Cohen–Wagner extrapolation plot (a_{hkl} vs $\cos\theta\cot\theta$), preferred grain orientation was characterized by the Harris texture indices and ω scans. XRD line broadening was evaluated simply by integral breadths (β) and FWHM's in terms of the Williamson–Hall (WH) plots (β vs $\sin\theta$). The correction for instrumental broadening was performed with the aid of NIST LaB_6 standard and the Voigt function method. Then the modified WH method was used for the determination of coherent domain size and dislocation density (lattice microstrains).

III. RESULTS AND DISCUSSION

A. As-prepared state

Using TEM we found the mean grain size in the as-prepared UFG Cu to be 150 nm. This value is slightly higher than 100 nm reported in Ref. 16. A similar difference was expected because the present specimens of UFG Cu were prepared by HPT under lower pressure than those studied in Ref. 16. It is reasonable to assume that higher pressure results in smaller grain size. The bright field TEM image of the as-prepared state is shown in Fig. 1. As can be seen in Fig. 1, the specimen exhibits fragmented structure with high angle misorientation of neighboring grains. ''Diffusion'' contrast on GB's testifies to the nonequilibrium state of the majority of GB's. Another TEM image of the as-prepared UFG Cu is shown in Fig. 2. It is clearly visible that the grains almost free of dislocations are separated by the regions along GB's with high dislocation density ($\sim 10^{15}\ m^{-2}$). The thickness

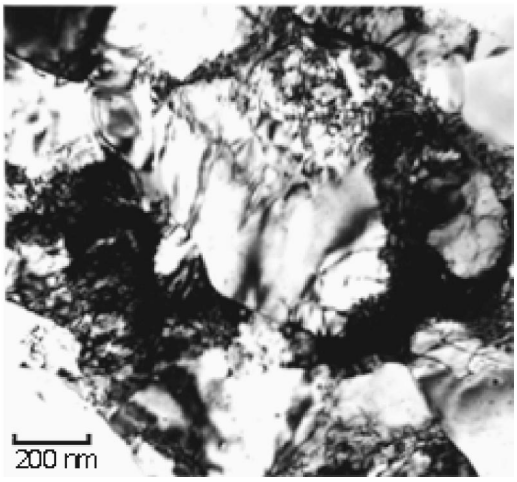

FIG. 1. Bright field TEM image of as-prepared state of UFG Cu.

of these distorted regions along GB's was observed to be ~ 20 nm, in agreement with Ref. 2. Rather complicated diffraction contrast inside the grains indicates high internal elastic stresses originating from the nonequilibrium GB's. The same features of the UFG structure were also reported in previous works.[16,17,2]

X-ray diffraction patterns show that the samples contain only pure fcc copper with the lattice parameter of 3.6151(4) Å, which very well corresponds to the value given in the PDF-2 powder diffraction pattern database.[26] Small preferred grain orientation of the type $\langle 100\rangle$ was detected. However, in most cases of the Cu samples obtained by HPT almost no texture was observed. Expected line broadening was observed, see Fig. 3. It indicated strains of about 0.1% and always showed significant characteristic anisotropy of the type $\beta_{h00} > \beta_{hhh}$. The anisotropy can be explained by dislocation-induced line broadening and the corresponding

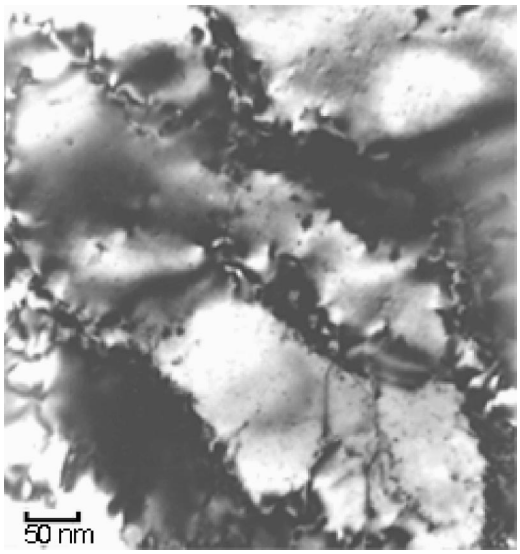

FIG. 2. Bright field TEM image of as-prepared state of UFG Cu. Magnification was increased compared to Fig. 1. Dislocation-free regions separated by the distorted ones with high dislocation density are clearly visible.

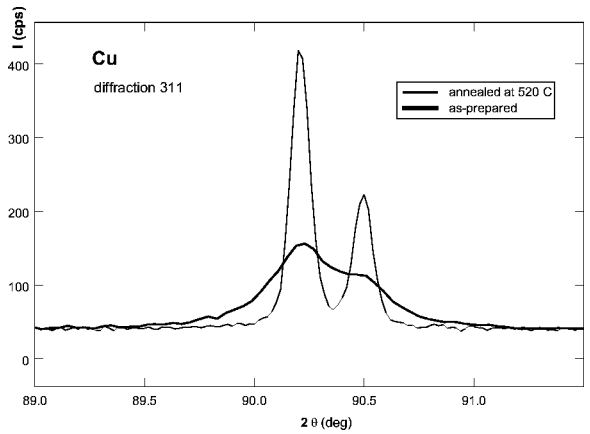

FIG. 3. XRD line profiles of the peak 311. The thick line corresponds to the as-prepared sample; the thin peak was obtained from the sample annealed up to 500 °C.

orientation (contrast) factors for the most common slip systems in the fcc structure (Burgers vector $\mathbf{b}=a/2\langle 110\rangle$) can be evaluated. A simple proposed procedure for the evaluation has been briefly described in Ref. 27 and will be published separately. The results are shown in Fig. 4 in terms of the well-known Williamson–Hall plot, the slope of which is proportional to the microstrain (or square root of dislocation density) and the intercept gives reciprocal value of the mean domain size. The agreement of experimental results and theoretical calculations is very good. The obtained values of domain size d and the mean dislocation density ϱ_D are 120 ± 20 nm and $(5\pm 2)\times 10^{14}$ m^{-2}, respectively.

The PL spectrum of the as-prepared specimen is well fitted by two exponential components (except for the two-component source contribution). The first component exhibits its lifetime $\tau_2 = 166 \pm 2$ ps and relative intensity $83 \pm 4\%$. The lifetime τ_2 is in good agreement with the lifetime $\tau_D \approx 164$ ps of positrons trapped at dislocations in deformed Cu.[28,29] Thus the component τ_2 represents the contribution of positrons trapped at dislocations.

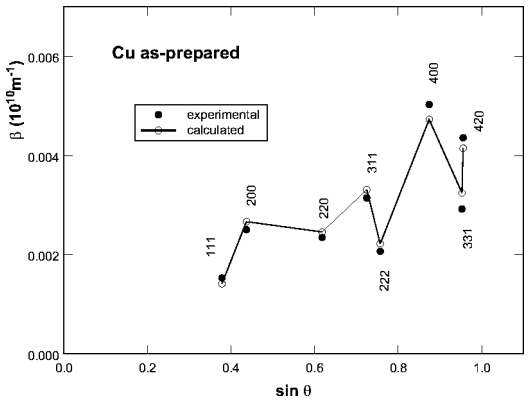

FIG. 4. Integral breadths (in reciprocal space units) vs sin θ. The closed circles correspond to the experimental values and open circles denote the values calculated for distribution of dislocations with the Burgers vector of $a/2\langle 110\rangle$, which are common for the fcc metals.

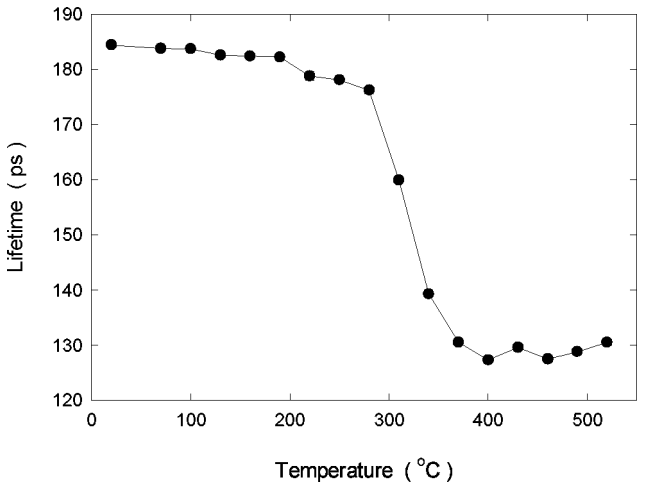

FIG. 5. The positron mean lifetime $\bar{\tau}$ as a function of annealing temperature.

In view of TEM observations, it is obvious that positrons are trapped at dislocations inside the DR's with high dislocation density which were found along GB's. We note that the mean grain size of the studied material is comparable to the mean diffusion length of free positrons, $L_+ \sim 150$ nm, in well-annealed Cu. Therefore, a relatively high fraction of positrons may reach the DR's and be trapped at dislocations inside them.

Migration of monovacancies was observed to start below 0 °C in plastically deformed[30] Cu or around 0 °C both in quenched[31] and electron irradiated[32] Cu. Thus, there is no contribution of positrons trapped in single monovacancies to the component τ_2. This conclusion is supported also by the remarkably shorter lifetime of this component compared to the lifetime $\tau_V = 180$ ps of positrons trapped in Cu monovacancy.[33] Moreover, high temperature stability of the component τ_2 with no changes of the lifetime during annealing (see Sec. III B, Figs. 5 and 6) testifies to this component as contribution of positrons trapped at dislocations inside the DR's.

Dislocation lines themselves represent relatively shallow traps for positrons with binding energy not greater than 0.1 eV.[34,35] Thus, it is generally accepted that positrons trapped at shallow trap of a dislocation diffuse rapidly along the line and are eventually trapped and annihilate in point defects associated with the dislocation.[34–36] That is why the lifetime of trapped positrons in deformed metals is only slightly lower than that of positrons trapped in monovacancies. Dislocations lines act as precursor states for transitions into deeper traps.

The second component resolved in the PL spectrum exhibits the lifetime $\tau_3 = 252 \pm 3$ ps and it may therefore be attributed to positron trapping in larger point defects with free volume comparable to that of a few monovacancies, see Sec. III C. Thus, we consider this component as the contribution of positrons trapped at microvoids, which were formed in the material due to strong deformation.

No component coming from delocalized positrons was found in the PL spectrum. Hence, all positrons in the specimen annihilate from the trapped state at a dislocation or in a

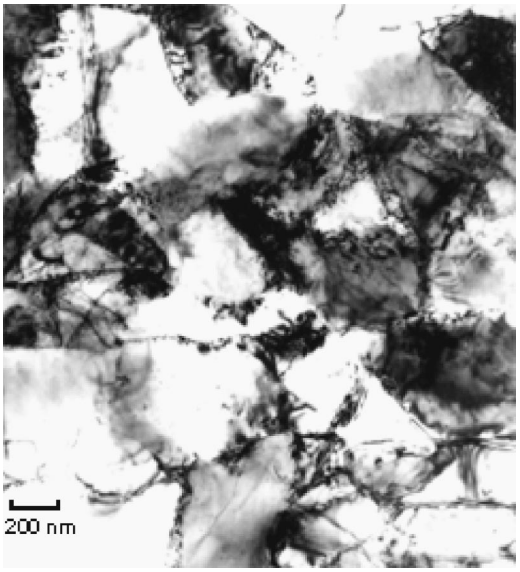

FIG. 6. The bright field TEM image of UFG Cu annealed up to 130 °C. No recovery of microstructure was found.

microvoid. It is not surprising because the mean diffusion length of positron is comparable with the mean grain size.

Note that a similar shape of the PL spectrum was found on UFG Cu prepared by HPT which was subjected to heating at 175 °C for 0.5 h prior to measurement.[14] Contrary to some NC materials prepared by GCM (Refs. 13 and 12) no positronium formation occurs in the specimen studied. It is a direct indication that no pores with size greater than 10 nm are present in the specimen.

B. Isochronal annealing

It is known that the positron mean lifetime $\overline{\tau}$ is a robust parameter which does not depend on the number of components to which a PL spectrum is decomposed. Therefore, we first use this parameter for a description of changes which occur during annealing. The mean lifetime for UFG Cu is plotted in Fig. 5 as a function of the annealing temperature.

Clearly, no change of $\overline{\tau}$ occurs up to 160 °C. One can recognize two annealing steps in Fig. 5: (i) a slight drop of $\overline{\tau}$ in the temperature interval 160–250 °C and (ii) a dramatic decrease of $\overline{\tau}$ from 280 up to 400 °C. The mean lifetime does not exhibit further changes above 400 °C. It seems to be straightforward that the above-mentioned annealing stages are connected with some recovery processes of the initial microstructure.

In order to obtain detailed information about microstructure changes, TEM observations were performed at selected temperatures. Bright field TEM image of the specimen annealed up to 130 °C is shown in Fig. 6. One can see virtually the same features of the microstructure as on the as-prepared state. Therefore, we conclude that no observable changes of the microstructure take place up to this temperature. On the other hand, significant changes of the microstructure were observed by TEM on the specimen annealed up to 190 °C, see Fig. 7. This temperature corresponds to

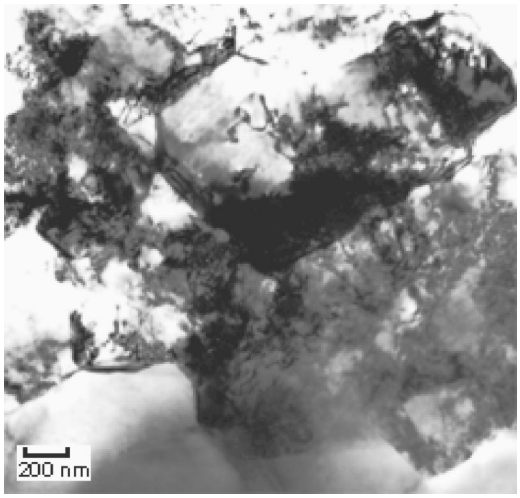

FIG. 7. The bright field TEM image of UFG Cu annealed up to 190 °C. Isolated recrystallized grains appear in the specimen, while the remaining deformed matrix remains essentially unchanged.

annealing stage (i). Relaxation of internal stresses inside the grains was observed at this temperature. In addition, abnormal grain growth of isolated grains, which are almost free of dislocations [dislocation density $(1–5)\times 10^{12}$ m^{-2}], takes place in a deformed matrix. A similar picture can be seen in Fig. 8, which corresponds to the specimen annealed up to 250 °C. The mean linear size of these recrystallized grains is from 2 to 3 μm. Annealing twins were observed inside the recrystallized grains. At the same time the mean cell size in the deformed matrix remains essentially unchanged.

Bright field TEM image of the specimen annealed up to 280 °C, which represents the onset of annealing stage (ii), is shown in Fig. 9. Recrystallization, i.e., grain growth in whole volume of the sample, occurs during this stage. The deformed matrix is consumed by almost defect-free recrystallized grains. The mean linear size of recrystallized grains is

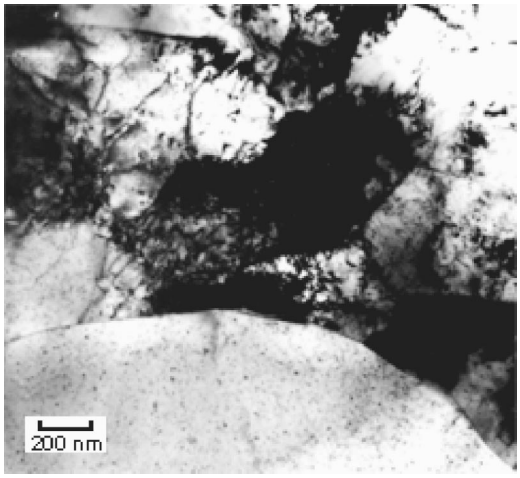

FIG. 8. The bright field TEM image of UFG Cu annealed up to 250 °C. The interface between an abnormally grown grain and the deformed matrix is clearly visible. The small black dots are only artifacts of ion milling of the specimen prior to measurement.

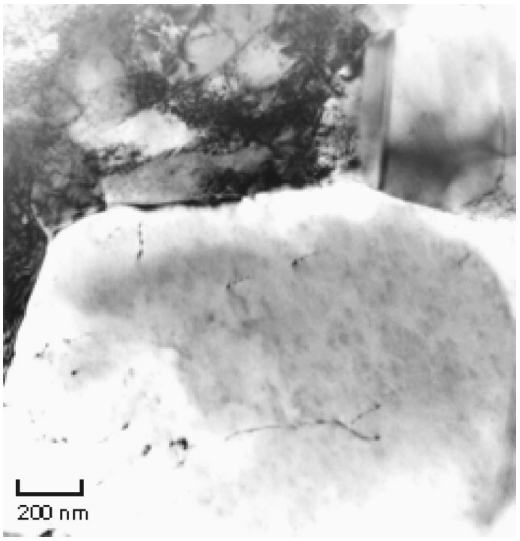

FIG. 9. The bright field TEM image of UFG Cu annealed up to 280 °C. The recrystallization occurs in the specimen at this annealing temperature.

~ 3 μm. Their volume fraction lies in the range from 20% to 30% at 280 °C and increases to an interval from 40% to 50% at 310 °C.

Fully recrystallized material is shown in Fig. 10, which is a TEM image of the specimen annealed up to 400 °C. The recrystallized grains with linear size of 3 μm prevail, however the grains with sizes from 1 to 10 μm were found. The recrystallized grains contain the annealing twins, see Fig. 10. The mean dislocation density in the recrystallized specimen

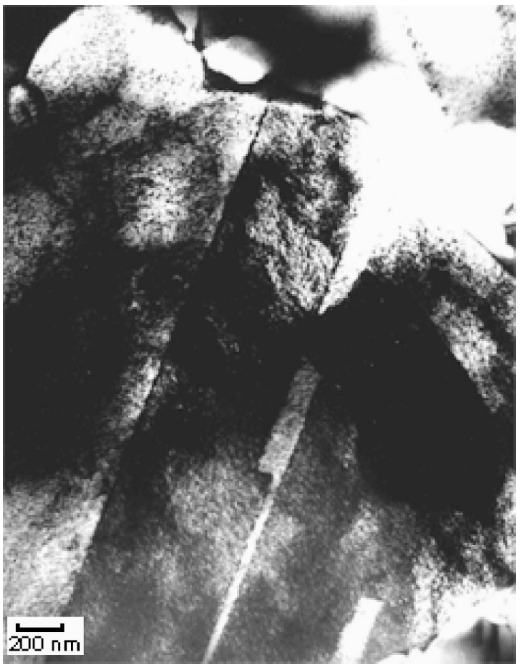

FIG. 10. The bright field TEM image of UFG Cu annealed up to 400 °C. The specimen exhibits a fully recrystallized microstructure. The small black dots are only artifacts of ion milling of the specimen prior to measurement.

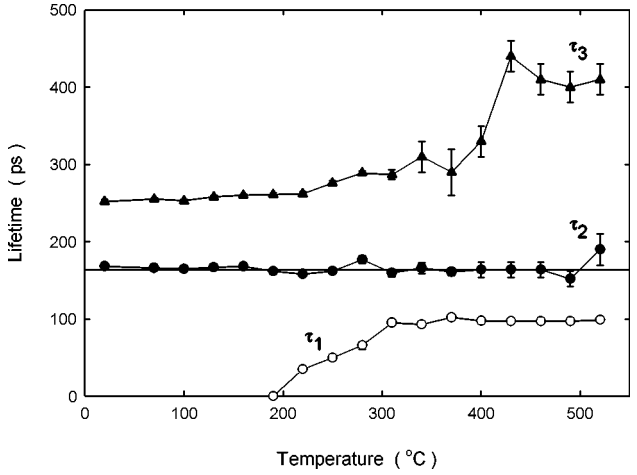

FIG. 11. The lifetimes of exponential components found in PL spectra of UFG Cu as a function of annealing temperature. The fixed value of the lifetime τ_2, see the text, is indicated by the solid line, while the closed circles correspond to lifetimes τ_2 obtained from an unconstrained fit.

lies around 10^{12} m^{-2}. Virtually the same picture was found also at higher temperatures than 400 °C. Hence, on the basis of the present TEM study, we attribute annealing stage (i) to the abnormal grain growth, where isolated almost dislocation-free grains appear in the deformed matrix, and stage (ii) to the recrystallization. XRD studies on the sample annealed up to 520 °C gave lattice parameter of 3.6148(3) Å corresponding to the ideal value. Small preferred orientation was of type 311 but the development of texture was not systematically studied on the same specimen. Diffraction linewidths nearly corresponded to the instrumental broadening (Fig. 3) so that no microstructural analysis from XRD was possible. It indicates only low strain in the specimen and grains larger than a few hundreds nanometers.

Our results exhibit very good consistency with the study of UFG Cu performed recently by Islamgaliev *et al.*[17] In that work UFG Cu was heated with constant effective heating rate of 20 °C/min. It is well known that a higher heating rate often leads to a shift of recovery processes to somehow higher temperatures. No noticeable grain growth was found by the authors in Ref. 17 up to 185 °C. Start of the abnormal grain growth was found at 220 °C and the appearance of annealing twins inside the grains was also reported.[17] In agreement with our observation, the mean linear size of the recrystallized grains from 2 to 2.5 μm was recently found by other authors.[17]

For further analysis the PL spectra at each annealing temperature were decomposed into exponential components corresponding to individual annihilation sites of positrons. Except for the source contribution, the measured PL spectra were well fitted by two exponential components up to 200 °C. Three components were found at higher annealing temperatures, due to the occurrence of the free positrons contribution with lifetime τ_1.

The lifetimes of individual spectral components as functions of annealing temperature are plotted in Fig. 11. Corresponding relative intensities are given in Fig. 12. As one can

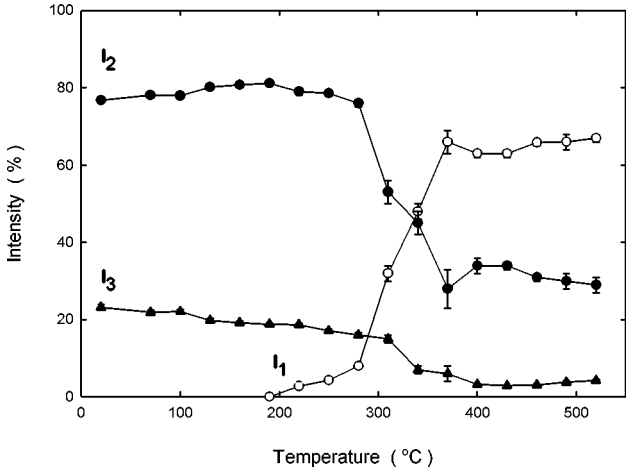

FIG. 12. Dependence of the relative intensities of individual components on annealing temperature.

see in Fig. 11, the lifetime τ_2 exhibits no temperature dependence except for fluctuations around the mean value of 164 ± 1 ps. Therefore, the lifetime τ_2 was fixed at 164 ps and all the PL spectra were subsequently refitted with this constraint in order to reduce statistic uncertainties and mutual correlations of other fitted parameters. The lifetimes τ_1, τ_3 and the relative intensities shown in Figs. 11 and 12 were obtained from this second decomposition. Only the results of this second decomposition will be used in the following analysis.

No contribution of free positrons was found in the PL spectra below 200 °C (see Figs. 11 and 12). Thus all positrons are trapped at defects up to 200 °C. The component with lifetime $\tau_1 < 100$ ps coming from free positrons was, however, clearly resolved in the PL spectra of the specimen annealed at higher temperatures above 200 °C (see Figs. 11 and 12). The contribution of free positrons appeared in the PL spectra at annealing stage (i), when the abnormal grain growth occurs. The recrystallized grains are almost free of dislocations and also lower concentration of the microvoids inside them is expected. Therefore the appearance of component τ_1 in stage (i) seems to be due to annihilations of free positrons inside the isolated recrystallized grains.

C. Microvoids

Special attention has to be focused on the microvoids. We note that an important benefit of using PL spectroscopy in the study of the present material consists in its ability to bring valuable information regarding the microvoids (concentration, mean size), which can hardly be provided by other techniques.

The microvoids were rarely observed on the UFG Cu specimens by TEM inside the regions free of dislocations. A typical example is shown in Fig. 13. On the basis of these observations the diameter of the microvoids was estimated to lie below ~ 10 nm.

Evaluation of the size of the microvoids can, however, much more precisely be made by PL spectroscopy. The lifetime τ_3 clearly indicates that the open volume of the microvoids exceeds that of the monovacancy. Therefore, dependence of positron lifetime on the size of a cluster of vacancies was calculated in the present work for Cu. We follow the lifetime calculations[37] of this dependence already made in the literature for other elements, e.g., Al and Ni. The positron potential was constructed from the lattice Coulomb potential and the electron-positron correlation potential which depends on the electron density.[38] The crystalline charge density and Coulomb potential were approximated by superimposing the densities and Coulomb potentials of free atoms, respectively.[37] The Schrödinger equation for positrons was solved on a three-dimensional grid using a conjugate gradient method.[39] In this way, the ground state positron energy and wave function, ψ_+, were obtained. The positron annihilation rate was determined from the equation[38]

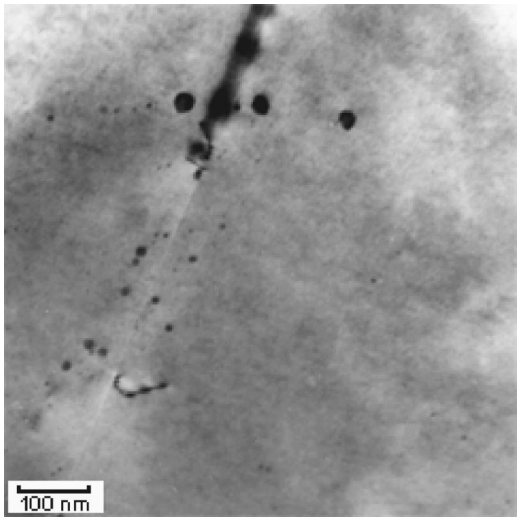

FIG. 13. The bright field TEM image of UFG Cu annealed up to 190 °C. The image was taken inside of some abnormally grown grain. One can see a few microvoids in the grain.

$$\lambda = \pi r_0^2 c \int n_+(\mathbf{r}) n_-(\mathbf{r}) \gamma[n_-(\mathbf{r})] d\mathbf{r}, \qquad (1)$$

where r_0 is the classical electron radius and c is the speed of light. The symbols $n_-(\mathbf{r})$ and $n_+(\mathbf{r}) = |\psi_+(\mathbf{r})|^2$ denote the electron and positron density, respectively. The enhancement factor γ reflects enhancement of the electron density at the site of positron, which is due to the attractive electron-positron interaction. In the present calculations we used the form of γ introduced by Boroński and Nieminen[40] as well as that suggested by Stachowiak and Lach.[41,42]

The calculations were performed using the 256 atom based supercells considering periodic boundary conditions for the positron wave function. Recent investigations regarding the convergence of calculated positron parameters with respect to the supercell size indicate that the supercells used in the present calculations are sufficiently large to obtain well-converged results.[43]

Stable vacancy cluster configurations were determined using the results of theoretical calculations performed by Johnson[44] for fcc metals. No relaxation of atoms surrounding

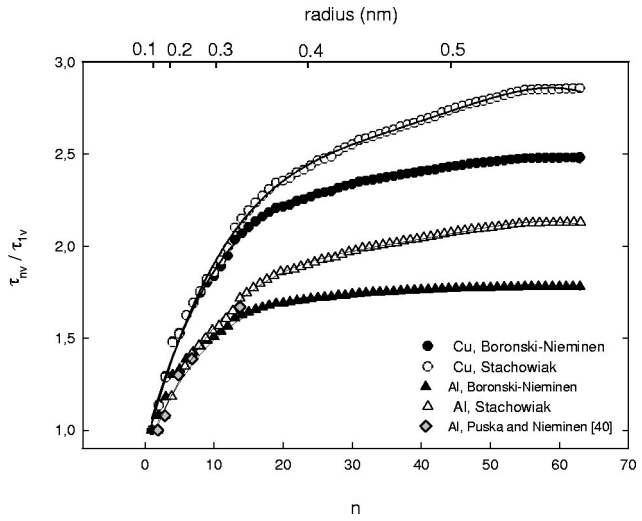

FIG. 14. The calculated dependence of the ratio of positron lifetime τ_{nv} in cluster consisting from n vacancies to the lifetime τ_{1v} (for monovacancy) on n. The corresponding radius of a cluster is indicated in the upper axis. The results obtained using Boroński–Nieminen's (closed circles) and Stachowiak's (open circles) enhancement factor are compared. In addition to the results for Cu, the calculated dependence τ_{nv}/τ_{1v} is shown for Al again using Boroński–Nieminen's (closed triangles) and Stachowiak's (open triangles) enhancements in order to compare our results with that calculated by Puska *et al.* (Ref. 37) gray diamonds. The solid lines represent fit of the dependence by fourth-order polynomial function, see the text.

the clusters was taken into account, as it is known that it has a very small influence on calculated positron lifetimes in fcc metals.[37]

The results of the calculations are shown in Fig. 14, where the ratio of the lifetime τ_{nv} of positron trapped in a cluster consisting of n vacancies to the lifetime τ_{1v} of positron trapped in a monovacancy is plotted versus n.

The results obtained using Boroński–Nieminen's and Stachowiak's enhancement factor, respectively, are compared in Fig. 14. The lifetime $\tau_{1v}=168$ ps was calculated for positron trapped in a monovacancy in Cu using Boroński–Nieminen's enhancement factor. It is in relatively good agreement with the experimental value of 180 ps.[33] On the other hand, Stachowiak's form of γ leads to lower value $\tau_{1v}=157$ ps. One can see in Fig. 14 that τ_{nv}/τ_{1v} saturates substantially slower in the case of the enhancement factor from Ref. 40. This is due to improper behavior of this enhancement factor for very low electron densities.[45] Stachowiak's form of γ exhibits more correct behavior for very low electron densities,[41,42] which leads to faster increase of the τ_{nv}/τ_{1v} ratio. Therefore, we use the results obtained with Stachowiak's enhancement in further discussion. Note that the difference between free volumes determined using the two various enhancements is smaller than 20%.

In addition to Cu, the dependence of τ_{nv}/τ_{1v} on n was calculated also for Al, see Fig. 14, with aim to compare our results with the previous calculations for Al.[37] One can see in Fig. 14 that there is good agreement of the ratio τ_{nv}/τ_{1v} calculated in the present work for Al with the previous

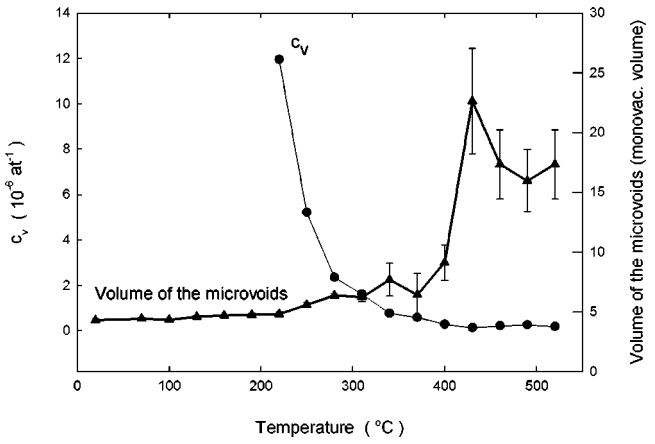

FIG. 15. The dependence of the open volume of the microcavities on the annealing temperature. The open volume was obtained using Eq. (2). The mean concentration of the microvoids c_v as a function of the annealing temperature is also included. The mean concentration c_v was determined using the model introduced in the present work.

work,[37] despite the fact that the lifetimes τ_{nv} calculated in the present work are slightly lower than those given in Ref. 37. This difference originates from a different formula for parametrization of the enhancement factor γ in Ref. 37. However, it does not affect the relative increase of lifetime with the size of cluster. It is illustrated in Fig. 14, where the τ_{nv}/τ_{1v} ratio calculated in Ref. 37 is also included.

The dependence of τ_{nv}/τ_{1v} on n can be well approximated (within 5% uncertainty, see the solid lines in Fig. 14) by polynomial function

$$\tau_{nv}/\tau_{1v}=an^4+bn^3+cn^2+dn+e. \qquad (2)$$

For Cu we obtained $a=(-5.3\pm0.4)\times10^{-7}$, $b=(8.6\pm0.5)\times10^{-5}$, $c=(-5.1\pm0.2)\times10^{-3}$, $d=(1.36\pm0.03)\times10^{-1}$, and $e=0.93\pm0.1$.

The open volume of the microvoids, expressed in units of the monovacancy open volume, derived from the lifetime τ_3 using the results of the present calculations, as a function of the annealing temperature is shown in Fig. 15. The open volume of the microvoids in the as-prepared state corresponds to that of about 5 monovacancies. As one can see in Fig. 15, it remains approximately constant up to 200 °C and then increases gradually to the open volume corresponding to ~8 monovacancies in the temperature range from 200 to 400 °C. Subsequently between 400 and 430 °C the open volume abruptly increases up to that of about 20 monovacancies.

We assume that some size distribution of the microvoids is present in the material. The mean value of this distribution corresponds to the open volume plotted in Fig. 15. Only the largest microvoids from this distribution may be observed by TEM. Decrease of concentration of the microvoids (reflected by a decrease of I_3) is accompanied by change of center of mass of their size distribution seen as increase of τ_3. The decrease of I_3 directly indicates that the concentration of the microvoids in the recrystallized grains is substantially lower

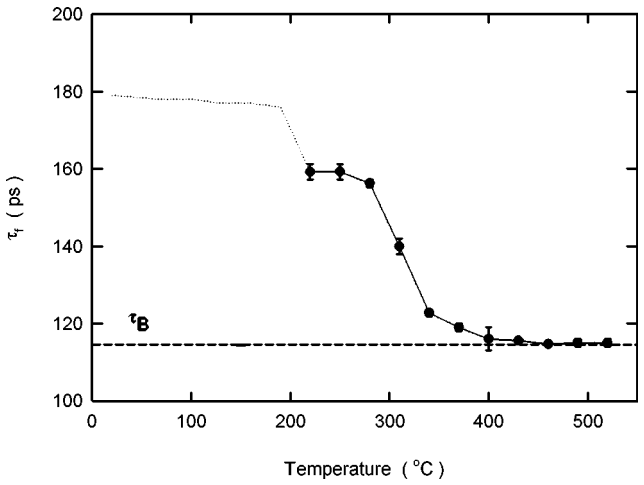

FIG. 16. Dependence of τ_f on annealing temperature. The dotted line at temperatures below 200 °C was obtained by formal use of Eq. (4) in the temperature range where saturated trapping occurs, indicating saturated trapping of positrons at defects. The dashed line shows the bulk lifetime τ_B of positrons in copper.

than inside the initial NR's. It seems to be most probable that small microvoids disappear preferentially in the recrystallized grains.

IV. FURTHER ANALYSIS OF THE RESULTS

The simple trapping model (STM)[46] is often used in further analysis of PL spectra because it allows for a determination of positron trapping rates and thereby concentrations of present type of defects. Nevertheless, it should be pointed out that the STM is based on some assumptions which may or may not be valid for the measured specimen. The assumptions can be summarized as follows:

(i) the annihilation rates of positrons trapped at the same kind of defect are the same,

(ii) only thermalized positrons can be trapped, and

(iii) the defects are distributed homogeneously.

In order to test the validity of the above-mentioned assumptions and thereupon applicability of the STM for a given specimen it is convenient to define the quantity

$$\tau_f = \left(\sum_i I_i / \tau_i \right)^{-1}, \tag{3}$$

where τ_i and I_i ($\Sigma_i I_i = 1$) denote the lifetimes and relative intensities of the spectral components. In the frame of STM the relation

$$\tau_f = \tau_B \tag{4}$$

holds.[46] τ_B in Eq. (4) states the bulk positron lifetime, i.e., lifetime of free positrons in defect-free material. Obviously, relation (4) can be experimentally verified only when the free positron component is resolved in the measured PL spectrum.

The dependence of τ_f on annealing temperature is shown in Fig. 16. It is plotted only for temperatures higher than 200 °C, where validity of relation (4) can be tested. The behavior of τ_f at lower temperatures is indicated by a dotted line. It is clear at first sight that τ_f is substantially higher than τ_B (114 ps for Cu,[15] shown by the dashed line in Fig. 16) and, therefore, relation (4) fails for annealing temperatures below 400 °C. It is direct indication that some assumption of STM is not satisfied for the studied specimen. While assumption (i) is obviously valid and the validity of assumption (ii) may be the subject of some discussion, assumption (iii) is certainly incorrect because of the obvious inhomogeneity of spatial distribution of dislocations, which represent dominant positron traps in the specimen. Hence, it seems to be most probable that strongly nonhomogeneous spatial distribution of dislocations in the specimen bars STM from being applied in the present case.

It is evident from the above-presented discussion that a proper description of positron behavior in UFG Cu has to be made using a model which reflects the spatial distribution of defects in the material. Such a model was developed in the present work and is described in the following text.

Positron trapping at inhomogeneously distributed defects was discussed by a number of researchers.[47–49] Various developed models were applied to the PL study of deformed metals with cellular dislocation structure,[47] and positron trapping at grain boundaries.[49] However, the specimens of UFG Cu exhibit some specific features, which need not be considered for other materials. Namely, the volume fraction η of the DR's is significant (see Sec. I) and certainly cannot be neglected compared to the volume fraction of nondistorted ones. Moreover, the distance between the DR's is comparable to the positron diffusion length. Both of these features have to be incorporated in the model.

It is convenient to distinguish two different kinds of regions of the studied specimen of UFG Cu:

(i) distorted regions (DR's) along GB's (thickness $\delta \sim 20$ nm) with high density of dislocations ($\varrho_D \sim 10^{15}$ m^{-2}) and relatively high level of internal stresses, and

(ii) nondistorted regions (NR's) with low density of dislocations ($\varrho_D \sim 10^{12}$ m^{-2}).

We assume that positrons are trapped at dislocations *only* inside the DR's. This assumption is quite reasonable as dislocation density inside the DR's is at least two orders of magnitude greater than that inside the NR's. Dislocation density inside the NR's is in fact close to the lower limit of sensitivity of PL spectroscopy.[50]

Using TEM, we have found some rare microvoids inside the NR's. Estimation of the diameter of these microvoids leads to a value below 10 nm. We assume that there is some size distribution of the microvoids in the specimen. A few microvoids observed by TEM inside the NR's represent only the largest ones from the distribution. It is reasonable to assume that the microvoids are homogeneously distributed inside the NR's. There is in principle no reason why the microvoids cannot also be presented inside the DR's, however we would not be able to see them by TEM due to the presence of a large amount of dislocations. In order to determine whether the microvoids are also present inside the DR's, we used two approaches. (1) We consider that the microvoids

are situated inside the NR's only. The model developed under this assumption will be shown in the following text. (2) In addition, an alternative model was developed with consideration that the microvoids are homogeneously distributed throughout the *whole* material, i.e., also inside the DR's. The latter approach (2) is not described in the present paper. Contrary to model (1) shown here, model (2) leads to an unreasonablly small size of the NR's. For example, at a temperature of 220 °C we obtained the size of NR's of 80 and 4 nm using models (1) and (2), respectively. Thus, assumption (1)—that the microvoids are situated inside the NR's only—seems to be a much more realistic description of the studied specimen.

Hence, we obtain the following conditions for positron trapping: (i) inside DR a positron annihilates from the trapped state in a dislocation and (ii) inside NR a positron annihilates as trapped at a microvoid or from free state. No detrapping is considered.

After thermalization some (non-negligible) fraction of positrons will be situated inside the DR's. Clearly, the probability that a positron ends its thermalization inside the DR's equals the volume fraction of the DR's, η. As there is an extremely high concentration of defects inside the DR's, we assume that all positrons, which are thermalized inside the DR's, annihilate from trapped state at a dislocation. If a positron ends its thermalization inside a NR, it diffuses throughout the material until it is trapped or annihilates from a free state. Obviously, during its life in the specimen, it may reach some DR and be trapped inside. The mean linear size of NR is comparable to the positron diffusion length, therefore, diffusion of free positrons from the NR's to the DR's represents an important process. In order to model this process correctly, the diffusion equation for the positron inside the NR's has to be solved. In the present work we use an approach similar to that developed by Dupasquier *et al.*[49] for positron trapping at grain boundaries. However, important modifications of the approach regarding the specific features of UFG Cu mentioned previously were introduced.

The NR's were considered as spherical-shaped domains of radius R. The positron trapping occurs at the surface of the domains, i.e., inside the DR's. Constant thickness δ of the DR's was assumed. The volume fraction η of the DR's can be then expressed as

$$\eta = \frac{(R+\delta)^3 - R^3}{(R+\delta)^3}. \tag{5}$$

Detrapping of a positron already trapped at a dislocation or a microvoid is negligible. The space and time dependence of the positron density n is governed by the diffusion equation

$$\frac{\partial n}{\partial t} = D_+\left(\frac{\partial^2 n}{\partial r^2} + \frac{2}{r}\frac{\partial n}{\partial r}\right) - (\lambda_B + K_v)n, \tag{6}$$

where D_+ is the positron diffusion coefficient and K_v stands for the positron trapping rate to the microvoids.

The number of positrons trapped at the surface of a NR in unit time is

$$T = K_D 4\pi R^2 \delta n(R,t). \tag{7}$$

The symbol K_D represents the trapping rate to dislocations for a positron situated inside a DR. At the same time T equals the density gradient-driving current passing through the interface between the NR and the DR,

$$T = -4\pi R^2 D_+ \left(\frac{\partial n}{\partial r}\right)_{r=R}. \tag{8}$$

By combining Eqs. (7) and (8) one obtains the boundary condition for the diffusion Eq. (6),

$$\left(\frac{\partial n}{\partial r}\right)_{r=R} = -\frac{\alpha}{R} n(R,t). \tag{9}$$

The parameter

$$\alpha = \frac{K_D \delta R}{D_+} \tag{10}$$

was introduced in Ref. 49 and it characterizes the balance between capture-limiting factors. The limit $\alpha \to \infty$ corresponds to the diffusion-limited regime, while $\alpha = 0$ to the transition-limited capture.[49]

Contrary to Ref. 49, the fraction of positrons that completes the thermalization inside the DR's cannot be neglected in the present case. Thus, the initial condition for Eq. (6) has the form

$$n(r,0) = \frac{1-\eta}{4/3\pi R^3}. \tag{11}$$

As was discussed previously, positrons thermalized inside the DR's are quickly trapped at defects there. Thus only diffusion of positrons, which complete thermalization inside the NR's is considered. The analytical solution of (6) including the boundary and the initial conditions (9) and (11), respectively, is

$$n(r,t) = \frac{1-\eta}{4/3\pi R^3}\frac{R}{r}\sum_{k=1}^{\infty} a_k \frac{\sin(\beta_k r/R)}{\sin\beta_k} e^{-\lambda_k t}, \tag{12}$$

where β_k is the kth solution of

$$\beta_k \cot\beta_k + \alpha - 1 = 0, \tag{13}$$

$$a_k = \frac{2\alpha}{\beta_k^2 + \alpha(\alpha-1)}, \tag{14}$$

$$\lambda_k = \lambda_B + K_v + \frac{\beta_k^2 D_+}{R^2}. \tag{15}$$

By inserting the solution (12) into Eq. (7) or Eq. (8) one obtains the trapping rate $T(t)$ of positrons to dislocations inside the DR's.

The number N_f of free positrons can be obtained by spatial integration of the density $n(\mathbf{r},t)$,

$$N_f(t) = \oint n(\mathbf{r},t)d\mathbf{r} = 4\pi \int_0^R n(r,t)r^2 dr. \tag{16}$$

One obtains

$$N_f = 3(1-\eta)\alpha \frac{D_+}{R^2} \sum_{k=1}^{\infty} a_k \frac{1}{\lambda_k - \lambda_B - K_v} e^{-\lambda_k t}. \tag{17}$$

The rate equation describing the time evolution of the number N_D of positrons trapped in dislocations in the DR's is

$$\frac{dN_D}{dt} = -\lambda_D N_D + T, \tag{18}$$

where λ_D represents the annihilation rate of positron trapped at dislocation. The trapping rate

$$T = 3\frac{1-\eta}{R} K_D \delta \sum_{k=1}^{\infty} a_k e^{-\lambda_k t} \tag{19}$$

is obtained by inserting the solution (12) into Eq. (7). The initial condition

$$N_D(0) = \eta \tag{20}$$

reflects the fact that some fraction of positrons completes thermalization inside the DR's and is quickly trapped at dislocations. Solving Eqs. (18) and (20) gives

$$N_D = \eta e^{-\lambda_D t} + 3\alpha(1-\eta)\frac{D_+}{R^2} \times \sum_{k=1}^{\infty} a_k \frac{1}{\lambda_k - \lambda_D}(e^{-\lambda_D t} - e^{-\lambda_k t}). \tag{21}$$

The rate equation for the number of positrons trapped in the microvoids can be written as

$$\frac{dN_v}{dt} = -\lambda_v N_v + K_v N_f, \tag{22}$$

with the initial condition

$$N_v(0) = 0. \tag{23}$$

One obtains the solution

$$N_v = 3(1-\eta)\alpha \frac{D_+}{R^2} \sum_{k=1}^{\infty} a_k \frac{K_v(e^{-\lambda_v t} - e^{-\lambda_k t})}{(\lambda_k - \lambda_B - K_v)(\lambda_k - \lambda_v)}. \tag{24}$$

Hence, the lifetime spectrum

$$\mathcal{S}(t) = -\frac{d}{dt}(N_f + N_D + N_v) \tag{25}$$

takes the form

$$\mathcal{S}(t) = \sum_k^{\infty} \frac{1}{t_k} i_k e^{t/t_k} + \frac{1}{\tau_2} I_2 e^{t/\tau_2} + \frac{1}{\tau_3} I_3 e^{t/\tau_3}, \tag{26}$$

where

$$i_k = 3\alpha(1-\eta)\frac{D_+}{R^2} a_k \left(\frac{1}{\lambda_k - \lambda_B - K_v} - \frac{1}{\lambda_k - \lambda_D} - \frac{K_v}{(\lambda_k - \lambda_B - K_v)(\lambda_k - \lambda_v)} \right), \tag{27}$$

$$t_k = \left(\lambda_B + K_v + \frac{\beta_k^2 D_+}{R^2} \right)^{-1}, \tag{28}$$

$$I_2 = \eta + 3\alpha(1-\eta)\frac{D_+}{R^2} \sum_{k=1}^{\infty} a_k \frac{1}{\lambda_k - \lambda_D}, \tag{29}$$

$$\tau_2 = \frac{1}{\lambda_D}, \tag{30}$$

$$I_3 = 3\alpha(1-\eta)\frac{D_+}{R^2} \sum_{k=1}^{\infty} a_k \frac{K_v}{(\lambda_k - \lambda_B - K_v)(\lambda_k - \lambda_v)}, \tag{31}$$

$$\tau_3 = \frac{1}{\lambda_v}. \tag{32}$$

Clearly, infinitely many components cannot be resolved in spectra in any practical situation. Thus, we used three-component decomposition, where the first component represents weighted average

$$\tau_1 = \frac{\sum_{k=1}^{\infty} i_k t_k}{\sum_{k=1}^{\infty} i_k} \tag{33}$$

and the relative intensity

$$I_1 = \sum_{k=1}^{\infty} i_k. \tag{34}$$

The infinite sums in the above equations converge relatively fast. Therefore, the truncation at $k \geqslant \alpha$ turns out to be always acceptable.[49] On the basis of TEM observations, we assume $\delta \approx 20$ nm. Then we are able to determine the trapping rates K_D and K_v together with the radius of the NR's, R, from the experimental PL spectra. The dependence of the mean size of the NR's, $2R$, on the annealing temperature is shown in Fig. 17. For the as-prepared state of UFG Cu, we have obtained the mean linear size of the NR's of 80 ± 10 nm. This value is lower than the mean grain size of 150 nm determined by TEM. It is not surprising because PL spectroscopy directly reflects the change in dislocation density inside the DR's and the NR's, while TEM responses to different contrast in both kinds of regions. Thus, ''the size of the NR's'' does not necessarily mean ''the mean grain size,'' which is obtained by TEM. A similar difference was found[16] between ''the coherent domain size'' obtained using XRD profile analysis and ''the grain size'' observed by TEM in UFG Cu and Ni. ''The

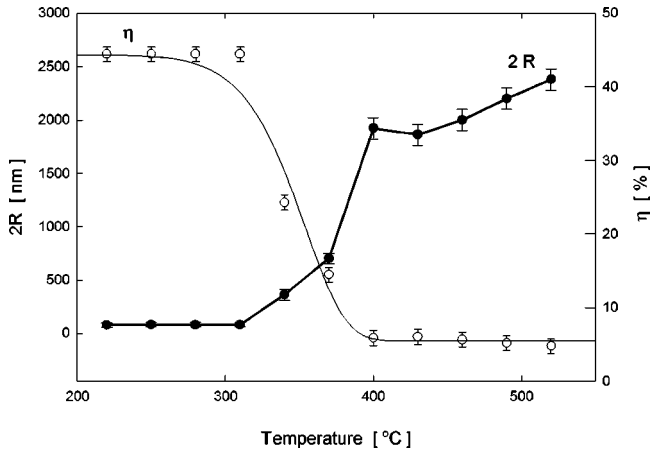

FIG. 17. The closed circle shows the dependence of the size of the NR's, $2R$, on annealing temperature. The open circle is the volume fraction η of the DR's as a function of annealing temperature. The results were obtained using the model for positron trapping in UFG material developed in the present work. The solid smooth line represents fit of temperature dependence of η by Eq. (39), which allows for determination of the activation energy of the recrystallization.

mean size of the NR's,'' $2R$, obtained by PL spectroscopy should correspond to ''the domain size'' determined by XRD, because both quantities are closely related to dislocation density. Indeed, ''the domain size'' of 120 ± 20 nm found in the as-prepared specimen, see Sec. III A, is lower than ''the mean grain size'' and exhibits relatively good agreement with $2R$. It should be pointed out that the assumption of spherical domain size for NR's was made in analysis of both the XRD and the PL spectra. As the actual shape of NR's is generally nonspherical, $2R$ should be treated as an effective linear size of the NR's. The geometrical significance of the effective linear size of nonspherical domains is addressed in Ref. 46. The good consistency of the R value obtained from our model both with the XRD and the TEM observations and the literature serves also as strong indirect evidence of the validity of the model used in the present work. Note that ''the mean grain size'' determined by TEM exhibits reasonable agreement with $2R$ obtained by PL spectroscopy, see Fig. 17, in the recrystallized material, i.e., above 400 °C, when the volume fraction of the DR's is negligible.

The mean size of the NR's, $2R$, remains practically constant up to 300 °C, see Fig. 17. It means that the abnormal grain growth affects only weakly the mean size of the NR's. Radical increase of $2R$ occurs during the recrystallization in the temperature range from 300 to 400 °C, see Fig. 17. Above 400 °C, $2R$ still gradually increases probably due to further growth of the recrystallized grains realized by migration of the high-angle GB's.

In addition to $2R$, the volume fraction η of the NR's calculated from Eq. (5) is plotted in Fig. 17 as a function of the annealing temperature. One can clearly see in Fig. 17 that η exhibits drastic decrease during the recrystallization (from 300 to 400 °C) where the DR's are consumed by the recrystallized grains.

Increase of volume fraction $X\equiv1-\eta$ of the recrystallized material with time t can be described by Göhler–Sachse's equation[51]

$$\frac{dX}{dt}\frac{1}{1-X}=K(T)(t-t_n)^{m-1}, \tag{35}$$

where t_n represents incubation time for nucleation and m is the kinetic exponent. The quantity K depends on temperature by Arrhenius equation

$$K=K_0\exp\left(-\frac{Q}{kT}\right), \tag{36}$$

where K_0 is a time-independent constant, k denotes the Boltzmann constant, and Q represents the activation energy of the recrystallization. The specimen was isochronally annealed, therefore, the effective heating rate $v_a=dT/dt$, remains constant. Thus, time in Eq. (35) may be expressed using temperature as

$$t=(T-T_s)/v_a, \tag{37}$$

where T_s denotes the annealing temperature, when the recrystallization starts. Inserting Eqs. (36) and (37) into Eq. (35), one obtains the following expression for the recrystallized fraction X:

$$1-X=\exp\left(-K_0\int\exp\left(-\frac{Q}{kT}\right)\left(\frac{T}{v_a}-t_1\right)^{m-1}dT\right), \tag{38}$$

where t_1 is another temperature-independent constant. In our case, the volume fraction of distorted regions, i.e., $1-X$, decreases from initial value η_1 to final value η_2, see Fig. 17. Thus, it is necessary to rescale Eq. (38), which leads to

$$\eta=(\eta_1-\eta_2)\exp\left(-K_0\int\exp\left(-\frac{Q}{kT}\right)\times\left(\frac{T}{v_a}-t_1\right)^{m-1}dT\right)+\eta_2, \tag{39}$$

where η is used instead of $1-X$. The integral on the right-side of Eq. (39) was solved numerically and the obtained function was fitted to temperature dependence of η obtained from experiment (Fig. 17). The function obtained from the fit is plotted in Fig. 17 by a solid line. One can see in Fig. 17 that the fitted function exhibits reasonable agreement with experimental points. The activation energy $Q=1.0\pm0.1$ eV (96 ± 10 kJ/mol) was determined from the fit. This value agrees well with the activation energy of 107 kJ/mol for migration of GB's in coarse-grained Cu.[52] Thus, it confirms that the annealing stage (ii) in our specimens occurs due to growth of the recrystallized grains. Analysis of the temperature dependence of microhardness for the UFG Cu revealed two stages with activation energy of 55 ± 10 and 98 ± 20 kJ/mol, respectively.[17] The later stage takes place between 300 and 350 °C and similar to our case it was attributed to the recrystallization.[17] Clearly, the activation energy for the growth of recrystallized grains determined by PL

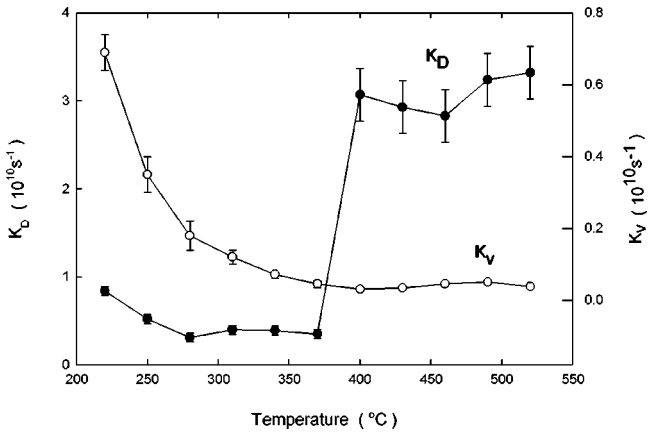

FIG. 18. The closed circle is the trapping rate K_D of positron situated inside DR to dislocations; the open circle is the positron trapping rate K_v to microvoids.

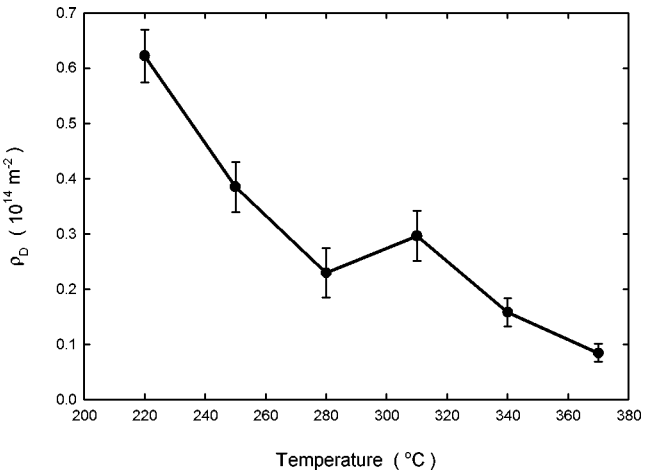

FIG. 19. The mean dislocation density ϱ_D for UFG Cu as a function of annealing temperature.

spectroscopy in the present work agrees well with that obtained from the microhardness measurements.[17]

The trapping rate K_D of positron situated inside DR to dislocation determined from our model [Eqs. (32)] is plotted in Fig. 18 as a function of annealing temperature. One can see in Fig. 18 that the trapping rate K_D decreases first up to 280 °C, i.e., in the stage of the abnormal grain growth. This decrease is likely caused by a decrease of dislocation density inside the DR's probably connected with some rearrangement of dislocations as was suggested also in Ref. 16. Then during the recrystallization K_D remains constant. However, for the recrystallized specimen at 400 °C it abruptly increases about one order of magnitude, see Fig. 18. The drastic increase of K_D can be explained only as the change of nature of positron traps in the recrystallized specimens. As was found by TEM, dislocation density in the recrystallized specimen lies around 10^{12} m^{-2}, which is the lower limit of sensitivity of PL spectroscopy.[50] Thus, positron trapping to dislocations becomes negligible in the recrystallized specimen and positrons are most probably trapped at high-angle boundaries of recrystallized grains.

Dislocation density inside the NR's is negligible compared to that inside the DR's. Hence, below 400 °C the mean dislocation density ϱ_D in the specimen is directly connected with the trapping rate K_D,

$$\varrho_D = \eta K_D / \nu_D, \tag{40}$$

where ν_D is the specific positron trapping rate to Cu dislocation. In the present work we used $\nu_D = 0.6 \times 10^{-4}$ m^2 s^{-1} determined by Čížek *et al.*[15] The mean dislocation density calculated from Eq. (40) is plotted in Fig. 19 as a function of annealing temperature. The mean dislocation density exhibits radical decrease in stage (i) of the abnormal grain growth. It is connected with the appearance of isolated dislocation-free recrystallized grains and also with the decrease of dislocation density, i.e., some rearrangement of dislocations, inside the DR's, which was reflected by a decrease of K_D. Further decrease of ϱ_D takes place during the primary recrystallization. The mean dislocation density in the as-prepared state of specimen cannot be determined by PL spectroscopy due to saturated trapping. However, one can see in Fig. 19 that ϱ_D certainly lies above 0.7×10^{14} m^{-2}. Saturated trapping requires the mean dislocation density in specimen above this value, as can be seen from the following simple estimation. Clearly, the trapping rate T has to exceed the bulk trapping rate λ_B, i.e., $T > \lambda_B$. Using Eq. (19) one can write

$$3\frac{1-\eta}{R} K_D \delta \sum_{k=1}^{\infty} a_k e^{-\lambda_k t} \geqslant \lambda_B. \tag{41}$$

It follows from Eqs. (11) and (12) that the infinite sum cannot be greater than 1. Thus K_D obeys the relation

$$K_D \geqslant \frac{\lambda_B R}{3\delta(1-\eta)}. \tag{42}$$

Hence, assuming $\eta \approx 0.4$ for the as-prepared UFG Cu one obtains the condition $K_D \geqslant 1.1\lambda_B$. Using Eq. (40), the estimation of the mean dislocation density in the as-prepared specimen is then $\varrho_D \geqslant 0.7 \times 10^{14}$ m^{-2}, which agrees well with 10^{14} m^{-2} obtained on the UFG Cu by TEM and XRD.[16] In the case of recrystallized specimen ($T \geqslant 400$ °C), the trapping rate to grain boundaries can be expressed as

$$K = \nu_{\mathrm{GB}} \sigma, \tag{43}$$

where σ represents the specific surface of GB's. For spherical grains of diameter R, $\sigma = 3/R$. The quantity ν_{GB} is the specific positron trapping rate per unit specific surface. For the UFG Cu we obtained $\nu_{\mathrm{GB}} = (1.1 \pm 0.2) \times 10^4$ m s^{-1}, which remains approximately constant from 400 to 520 °C. There is lack of the specific trapping rate ν_{GB} for Cu in the literature. However, Dupasquier *et al.*[49] found the values of ν_{GB} range from 0.2×10^4 m s^{-1} (for Zn alloys) to 3×10^4 m s^{-1} (for Al alloys). Although these specific trapping rates were determined for other materials, we conclude that at least an order of magnitude of ν_{GB} obtained for the UFG Cu in the present work agrees with those in Ref. 49. It supports our assumption of positron trapping at GB's in the recrystallized specimen.

The trapping rate K_v of positron to the microvoids is directly connected with their concentration. Clearly, the mean concentration of the microvoids is

$$c_v = (1-\eta)K_v/\nu_v, \tag{44}$$

where ν_v represents the specific positron trapping rate to the microvoids. The specific trapping rate ν_v depends strongly on the size of a microvoid. For small spherical clusters consisting of n vacancies, ν_v can be approximated[46] by linear relation $\nu_v \approx n\nu_{1v}$, where $\nu_{1v} = 1.2 \pm 0.2 \times 10^{14}$ s^{-1} at. is the specifying trapping rate for Cu monovacancy.[53] The number of vacancies n corresponding to the open volume of a microvoid was calculated using Eq. (2). The mean concentration of the microvoids is then plotted as a function of annealing temperature in Fig. 15. One can see that the number of the microvoids decreases drastically from 220 to 350 °C, while the mean volume of the microvoids gradually increases. In the temperature interval from 370 to 430 °C the mean volume of the microvoids, however, drastically increases. At the same time c_v exhibits only relatively small monotonic decrease. Thus, the radical decrease of the microvoid concentration occurs during the abnormal grain growth. It seems to indicate that the recrystallized abnormally grown grains contain a substantially smaller number of the microvoids. It is expected that the smaller a microvoid, the smaller its thermal stability. Hence, the smallest microvoids disappear first from the material. It is reflected by a gradual shift of the mean volume of microvoids toward higher values, see Fig. 15. The mean volume of microvoids exhibits an abrupt increase at the end of the recrystallization stage. In this temperature range c_v decreases only moderately. Thus, only the largest (most stable) microvoids survive in the recrystallized specimen.

V. COMPARISON OF PL RESULTS WITH OTHER TECHNIQUES

An interesting point represents comparison of PL results with those obtained by other nonlocal techniques commonly used in investigations of thermal stability of NC and UFG metallic specimens, namely electrical resistivity and microhardness measurements. We compare the results obtained on UFG copper by PL spectroscopy in the present work with the electrical resistivity and the microhardness results on the same material published in Ref. 16. Results obtained by all the techniques are correlated in Fig. 20. The positron mean lifetime $\bar{\tau}$ is used as an integral parameter characterizing the PL spectrum. The mean lifetime $\bar{\tau}$ is plotted in Fig. 20 as a function of the electrical resistivity (solid line) and the microhardness (dotted line) obtained for the same annealing temperature indicated by the numbers in the vicinity of the individual points. There is no change detectable by any of the methods up to the annealing temperature of 150 °C. At higher annealing temperatures up to 250 °C (abnormal grain growth) the electrical resistivity as well as the microhardness exhibit a strong decrease, see Fig. 20. On the other hand, the mean lifetime $\bar{\tau}$ remains almost unchanged. Practically opposite behavior can be seen at temperatures above 250 °C

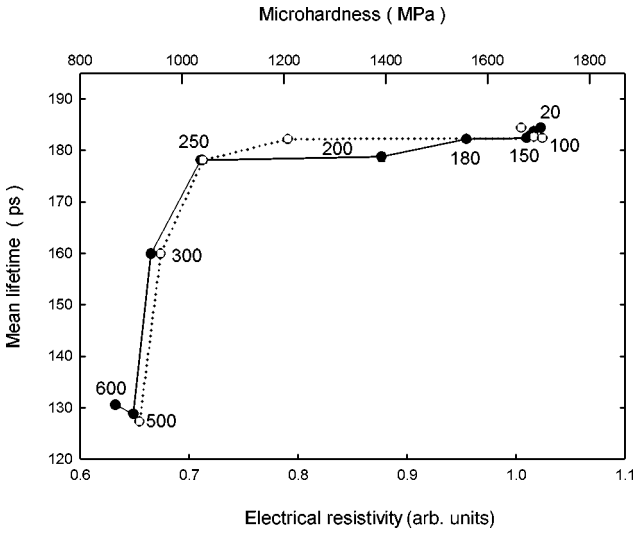

FIG. 20. Correlation of the mean positron lifetime $\bar{\tau}$ with the electrical resistivity and the microhardness. The mean positron lifetime $\bar{\tau}$ is plotted as a function of the electrical resistivity in arbitrary units (closed circle, solid line) and the microhardness (open circle, dotted line) obtained for the same annealing temperature indicated in centigrades by the numbers shown near the points. The electrical resistivity and the microhardness data were taken from Ref. 16.

(recrystallization), when $\bar{\tau}$ dramatically decreases, while the electrical resistivity and the microhardness exhibit only a slight decrease. The electrical resistivity and the microhardness exhibit very similar behavior, which is characterized by main decrease in the stage of the abnormal grain growth and relatively small decrease due to the recrystallization. The former decrease is probably connected with relaxation of elastic stresses as well as some rearrangement of dislocations in the DR's.[16] On the other hand, PL sensitivity to the stresses in specimen as well as dislocation rearrangement in the DR's is relatively low, therefore, it responds mainly to the recrystallization, when disappearance of the defects takes place.

VI. CONCLUSIONS

Thermal stability of UFG copper was studied by means of PL spectroscopy correlated with TEM. The initial grain size of about 150 nm was found. Positrons are trapped at dislocations inside the distorted regions and also in the microvoids. There is some size distribution of the microvoids with the mean size of about 5 vacancies. No significant change of microstructure was observed up to 150 °C. In the temperature region from 150 to 280 °C abnormal grain growth takes place. Isolated recrystallized grains almost free of defects grow in the deformed matrix. The mean concentration of the microvoids decreases remarkably during the abnormal grain growth and simultaneously their mean size gradually increases. In the temperature range from 280 to 400 °C recrystallization takes place, where the deformed matrix is consumed by the recrystallized grains. As a result the distorted regions disappear, which is accompanied by significant diminution of dislocation density. At the end of the recrystalliza-

tion stage the mean size of the microvoids abruptly increases up to about 20 vacancies. Thus, only the largest microvoids survive in the recrystallized material. Above 400 °C the specimen is fully recrystallized and the mean grain size of about 3 μm was found. Positrons in the recrystallized specimen are trapped most probably at the grain boundaries.

Spatial distribution of defects in the studied UFG copper is highly nonuniform, which does not allow one to use the simple trapping model. Therefore, the trapping model, which takes into account the nonuniform defect distribution as well as positron diffusion between the different regions, was developed in the present work. This model properly describes positron behavior in the UFG copper. The model allows for determination of the mean coherent size, density of dislocations, concentration of microvoids, and volume fraction of the distorted regions. The results obtained by this model are in good agreement with independent TEM and XRD observations performed in the present work as well as study performed by other authors.[16] Moreover, using the model of positron trapping developed in the present work, the activation energy of the recrystallization of 96 ± 10 kJ/mol was determined. It corresponds to the activation energy of migration of equilibrium grain boundaries in coarse-grained Cu.

High resolution of the PL spectrometer used in the present work has enabled proper determination of lifetime and relative intensity, especially of the free positron component, which is crucial for application of the developed model.

ACKNOWLEDGMENTS

This work was financially supported by the Grant Agency of the Czech Republic (Contract No. 106/01/D049) and the Ministry of Education, Youth and Sports of the Czech Republic (MSMT CR) through Grants No. OC 523.50 and No. OC P3.150 (program COST).

[1] R. Birringer, Mater. Sci. Eng., A **117**, 33 (1989).
[2] R. Z. Valiev, A. V. Korznikov, and R. R. Mulyukov, Mater. Sci. Eng., A **168**, 141 (1993).
[3] R. Z. Valiev, R. S. Musalimov, and N. K. Tsenev, Phys. Status Solidi A **115**, 451 (1989).
[4] R. Z. Valiev, R. K. Islamgaliev, and I. V. Alexandrov, Prog. Mater. Sci. **45**, 103 (2000).
[5] R. Z. Valiev, Mater. Sci. Eng., A **234-236**, 59 (1998).
[6] R. Z. Valiev and R. K. Islamgaliev, in *Superplasticity and Superplastic Forming 1998*, edited by A. K. Ghosh and T. R. Bieler (The Minerals, Metals and Material Society, Warrendale, PA, 1998), p. 117.
[7] F. H. Froes and C. Suryanarayana, J. Met. **6**, 12 (1989).
[8] P. G. Sanders, J. R. Weertman, and J. G. Barker, J. Mater. Res. **11**, 3110 (1996).
[9] X. Zhu, R. Birringer, U. Herr, and H. Gleiter, Phys. Rev. B **35**, 9085 (1987).
[10] H.-E. Schafer, W. Eckert, O. Stritzke, R. Würschum, and W. Templ, in *Positron Annihilation*, edited by L. Dorikens-Vanpraet, M. Dorikens, and D. Segers (World Scientific, Singapore, 1989), p. 79.
[11] M. Eldrup, P. G. Sanders, and J. R. Weertman, Mater. Sci. Forum **255-257**, 436 (1997).
[12] R. Würschum, M. Scheytt, and H.-E. Schaefer, Phys. Status Solidi A **102**, 119 (1987).
[13] H.-E. Schaefer, R. Würschum, R. Birringer, and H. Gleiter, Phys. Rev. B **38**, 9545 (1988).
[14] R. Würschum, W. Greiner, R. Z. Valiev, M. Rapp, W. Sigle, O. Schneeweiss, and H.-E. Schaefer, Scr. Metall. Mater. **25**, 2451 (1991).
[15] J. Čížek, I. Procházka, P. Vostrý, F. Chmelík, and R. K. Islamgaliev, Acta Phys. Pol. A **95**, 487 (1999).
[16] R. K. Islamgaliev, F. Chmelík, and R. Kužel, Mater. Sci. Eng., A **237**, 43 (1997).
[17] R. K. Islamgaliev, N. M. Amirkhanov, J. J. Bucki, and K. J. Kurzydlowski, in *Investigations and Applications of Severe Plastic Deformation*, NATO Science Series 3: High Technology 80, edited by T. C. Lowe and R. Z. Valiev (Kluwer, Dordrecht, 2000), p. 297.
[18] I. V. Alexandrov, K. Zhang, A. R. Kilmametov, K. Lu, and R. Z. Valiev, Mater. Sci. Eng., A **234-236**, 321 (1997).
[19] S. Okuda and F. Tang, Nanostruct. Mater. **6**, 585 (1995).
[20] R. Z. Valiev, Nanostruct. Mater. **6**, 73 (1995).
[21] F. Bečvář, L. Lešťák, I. Novotný, I. Procházka, F. Šebesta, and J. Vrzal, Mater. Sci. Forum **175-178**, 947 (1995).
[22] F. Bečvář, J. Čížek, L. Lešťák, I. Novotný, I. Procházka, and F. Šebesta, Nucl. Instrum. Methods Phys. Res. A **443**, 557 (2000).
[23] F. Bečvář, J. Čížek, and I. Procházka, Acta Phys. Pol. A **95**, 448 (1999).
[24] I. Procházka, I. Novotný, and F. Bečvář, Mater. Sci. Forum **255-257**, 772 (1997).
[25] R. Kužel, DIFPATAN - program for powder pattern analysis. 1995. http://www.xray.cz/priv/kuzel/difpatan
[26] PDF-2, Powder diffraction pattern database, ICDD (International Centre for Diffraction Data), record number 04-0836.
[27] R. Kužel, J. Čížek, I. Procházka, F. Chmelík, R. K. Islamgaliev, and N. M. Amirkhanov, Mater. Sci. Forum (to be published).
[28] B. T. A. McKee, S. Saimoto, A. T. Stewart, and M. J. Scott, Can. J. Phys. **52**, 759 (1974).
[29] A. P. de Lima, C. Lopes Gil, D. R. Martins, N. Ayres de Campos, L. F. Menezes, and J. V. Fernandes, in Proceedings of the European Meeting on Positron Studies of Defects, Vol. 2, part 1, edited by G. Dlubek, O. Brümmer, G. Brauer, K. Hennig, Martin-Luther-Universität Halle-Wittenberg, Wernigerode, 1987, p. C1.
[30] A. van den Beukel, in *Proceedings of the International Conference Vacancies and Interstitials in Metals*, edited by A. Seeger, D. Schumacher, W. Schilling, and J. Diehl (North-Holland, Amsterdam, 1970), p. 427.
[31] I. Kanazawa, H. Murakami, and M. Doyama, Phys. Status Solidi A **103**, 403 (1987).
[32] S. Mantl and W. Trifthäuser, Phys. Rev. B **17**, 1645 (1978).
[33] H.-E. Schaefer, W. Stuck, W. Bauer, and F. Banhart, Mater. Sci. Forum **15-18**, 117 (1987).

[34] L. C. Smedskjaer, M. Manninen, and M. J. Fluss, J. Phys. F: Met. Phys. **10**, 2237 (1980).
[35] H. Häkkinen, S. Mäkinen, and M. Manninen, Phys. Rev. B **41**, 12 441 (1990).
[36] J. Čižek, I. Procházka, T. Kmječ, and P. Vostrý, Phys. Status Solidi A **180**, 439 (2000).
[37] M. J. Puska and R. M. Nieminen, J. Phys. F: Met. Phys. **13**, 333 (1983).
[38] J. Arponen and E. Pajane, Ann. Phys. (N.Y.) **121**, 343 (1979).
[39] D. G. Luenberger, *Optimization by Vector Space Methods* (Wiley, New York, 1968).
[40] E. Boroński and R. M. Nieminen, Phys. Rev. B **34**, 3820 (1986).
[41] H. Stachowiak, Phys. Rev. B **41**, 12 522 (1990).
[42] H. Stachowiak and J. Lech, Phys. Rev. B **48**, 9828 (1993).
[43] T. Korhonen, M. J. Puska, and R. M. Nieminen, Phys. Rev. B **54**, 15 016 (1996).
[44] R. A. Johnson, Phys. Rev. **152**, 629 (1966).
[45] S. Van Petegem, J. Kuriplach, M. Hou, E. E. Zhurkin, D. Segers, A. L. Morales, S. Ettanoussi, C. Dauwe, and W. Mondelaers, Mater. Sci. Forum (to be published).
[46] P. Hautojärvi and C. Corbel, in *Proceedings of the International School of Physics "Enrico Fermi,"* Course CXXV, edited by A. Dupasquier and A. P. Mills (IOS Press, Varenna, 1995), p. 491.
[47] A. Dupasquier, in *Positron Annihilation*, edited by P. G. Coleman, S. C. Sharma, and L. M. Diana (North-Holland, Amsterdam, 1982), p. 381.
[48] J. Dryzek, Acta Phys. Pol. A **95**, 539 (1999).
[49] A. Dupasquier, R. Romero, and A. Somoza, Phys. Rev. B **48**, 9235 (1993).
[50] G. Dlubek, Mater. Sci. Forum **13-14**, 15 (1987).
[51] F. von Göhler and G. Sachs, Z. Phys. **77**, 281 (1932).
[52] J. P. Hirth and J. Lothe, *Theory of Dislocations* (McGraw-Hill, New York, 1982).
[53] J.-E. Kluin and Th. Hehenkamp, Phys. Rev. B **44**, 11 597 (1991).